Size-Dependent Localization and Penetration of Ultrasmall Gold Nanoparticles in Cancer Cells, Multicellular Spheroids, and Tumors *in Vivo*

Keyang Huang,[†,∥] Huili Ma,[†,∥] Juan Liu,[†] Shuaidong Huo,[†,‡] Anil Kumar,[†] Tuo Wei,[†] Xu Zhang,[†] Shubin Jin,[†] Yaling Gan,[†] Paul C. Wang,[⊥] Shengtai He,[‡,*] Xiaoning Zhang,[§,*] and Xing-Jie Liang[†,*]

[†]CAS Key Laboratory for Biological Effects of Nanomaterials and Nanosafety, National Center for Nanoscience and Technology, No. 11, First North Road, Zhongguancun, Beijing, China 100190, [‡]School of Materials Science and Engineering, Tianjin Polytechnic University, Tianjin, China 300387, [§]Laboratory of Pharmaceutics, School of Medicine, Tsinghua University, Beijing, China 100084, and [⊥]Laboratory of Molecular Imaging, Department of Radiology, Howard University, Washington, D.C. 20060, United States. [∥]These authors contributed equally to this work.

ABSTRACT

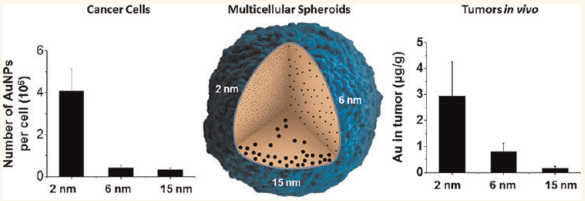

This work demonstrated that ultrasmall gold nanoparticles (AuNPs) smaller than 10 nm display unique advantages over nanoparticles larger than 10 nm in terms of localization to, and penetration of, breast cancer cells, multicellular tumor spheroids, and tumors in mice. Au@tiopronin nanoparticles that have tunable sizes from 2 to 15 nm with identical surface coatings of tiopronin and charge were successfully prepared. For monolayer cells, the smaller the Au@tiopronin NPs, the more AuNPs found in each cell. In addition, the accumulation of Au NPs in the *ex vivo* tumor model was size-dependent: smaller AuNPs were able to penetrate deeply into tumor spheroids, whereas 15 nm nanoparticles were not. Owing to their ultrasmall nanostructure, 2 and 6 nm nanoparticles showed high levels of accumulation in tumor tissue in mice after a single intravenous injection. Surprisingly, both 2 and 6 nm Au@tiopronin nanoparticles were distributed throughout the cytoplasm and nucleus of cancer cells *in vitro* and *in vivo*, whereas 15 nm Au@tiopronin nanoparticles were found only in the cytoplasm, where they formed aggregates. The *ex vivo* multicellular spheroid proved to be a good model to simulate *in vivo* tumor tissue and evaluate nanoparticle penetration behavior. This work gives important insights into the design and functionalization of nanoparticles to achieve high levels of accumulation in tumors.

KEYWORDS: ultrasmall gold nanoparticles · multicellular tumor spheroid · penetration behavior · drug delivery · cancer therapy

In the past decade, nanomedicine, owing to the unique advantages of nanoparticles over small molecules, has offered new strategies for cancer treatment. In the clinic, some commercially available nanomedicines such as Doxil (100 nm) and Abraxane (130 nm) have been shown to significantly reduce the side effects of the delivered drug due to the long circulation time and altered biodistribution of the particles. However, the therapeutic index increased to some extent because of limited drug delivery into the tumor tissue.[1,2]

The tumor microenvironment is structurally heterogeneous, containing for example clusters of tumor cells, nonuniform leaky vasculature, and a dense interstitial structure. This environment hinders the effective delivery of nanoparticles into tumors, especially into regions distant from the vasculature.[3,4] Overcoming these physiological barriers is a major challenge for the field of nanoparticle research.

Generally, the physical, chemical, and biological properties of nanoparticles affect the delivery capacity in different ways. Positively charged nanoparticles improve the delivery of payloads to the cells, whereas negatively charged nanoparticles diffuse more quickly, thereby delivering drugs into deep tissues.[5] It has been shown that nanorods penetrate tumors more rapidly than nanospheres due to improved transportation through pores.[6] Another study demonstrated significantly increased penetration (up to 100 nm) by collagenase-coated nanoparticles, owing to degradation of collagen in the extracellular matrix.[7] Decreasing the nanoparticle size may improve the delivery efficiency in tumor tissue.[5,8,9] In addition, it was reported that gold and silver nanoparticles (2−100 nm) coated with Herceptin (mAb) regulated membrane receptor internalization in monolayer cells.[10]

In recent years, colloidal chemistry and nanoscience have made great steps forward due to significant improvements in the controlled synthesis of nanostructures of

* Address correspondence to liangxj@nanoctr.cn; drugman@mail.tsinghua.edu.cn; sht-he@tjpu.edu.cn.

Received for review March 22, 2012 and accepted April 27, 2012.

Published online April 27, 2012
10.1021/nn301282m

© 2012 American Chemical Society

different sizes for biomedical application.[11] However, the exact effects of ultrasmall nanoparticles on tumor penetration are still not well understood. We previously showed that 2 nm AuNPs significantly improved the delivery of therapeutic peptides and targeted peptides into cancer cells. These ultrasmall functional nanoparticles showed high efficacy for cancer treatment.[12] We therefore hypothesized that smaller nanoparticles (those less than 10 nm) would have special advantages in terms of tumor penetration over larger nanoparticles.

Colloidal gold nanoparticles have great potential to overcome delivery limitations because of their biocompatibility, low toxicity, small size, and tunable surface functionalities.[13] The first clinical trial of gold nanoparticle related namomedicine, CYT-6091, is comprised of recombinant human tumor necrosis factor alpha (rhTNF) bound to the surface of PEGylated 27 nm colloidal gold nanoparticles,[14] and a phase I clinical trial in patients with advanced stage solid cancers showed the accumulation of gold nanoparticle in tumor tissue.[15] In addition, gold nanoparticles have been identified as promising candidates for delivery of various payloads such as drugs,[16,17] proteins or peptides,[12,18] and nucleic acids.[19−21] Synthesis of gold nanoparticles can be controlled to obtain nanoparticles with a wide range of sizes.[12,13] We designed and synthesized small AuNPs that have tunable sizes from 2 to 15 nm with identical surface coatings and charge. We then systematically evaluated the size-dependent localization and penetration of 2, 6, and 15 nm spherical gold nanoparticles in monolayer breast cancer cells, a MCF-7 tumor spheroid model, and *in vivo* tumor tissue in mice. *Ex vivo* multicellular models have become the most commonly used tools to evaluate drug or nanoparticle penetration into tumors.[22−24] We therefore established a breast tumor spheroid model system to compare the size-dependent effects and penetration behaviors of 2−15 nm spherical gold nanoparticles. To evaluate the same phenomenon *in vivo*, we studied the distribution of Au nanoparticles in tumor-bearing mice.

RESULTS AND DISCUSSION

Synthesis and Characterization of Tiopronin-Coated AuNPs with Sizes from 2 to 15 nm. In order to investigate the size-dependent localization and penetration behavior of ultrasmall gold nanoparticles in breast cancer cells, multicellular spheroids, and tumor tissue, we synthesized tiopronin-coated gold nanoparticles with sizes ranging from 2 to 15 nm. Tiopronin is a very well known pharmaceutical drug, with established biocompatibility, which is used for the treatment of cystinuria and rheumatoid arthritis.[25] Au@tiopronin NPs of 2 and 6 nm were directly prepared by the protecting agent tiopronin with sodium borohydrate as reducing agent.[26]

Au@tiopronin NPs of 15 nm were obtained by surface exchange of tiopronin with corresponding Au@citrate NPs. The mechanism for this exchange is the higher binding affinity of tiopronin thiol groups for gold compared to the electrostatic interaction with citrate. Replacement of citrate by the thiol ligand of tiopronin did not affect the formation of the core of the gold nanoparticles, as shown in TEM images (Figure S1). The zeta potential of the nanoparticles decreased from −23.8 eV to −35.3 eV. X-ray photoelectron spectroscopy (XPS) indicated that the molar ratio of S to Au in the 15 nm Au@tiopronin nanoparticles was 0.22, and a similar molar ratio of N to Au was also observed (Figure S1). In addition, there was no significant difference between the visible spectrum and XRD profiles of Au@citrate and Au@tiopronin NPs (Figure S2), indicating that 15 nm Au@tiopronin NPs had been successfully prepared using this method.

The sizes of the Au@tiopronin NPs were characterized by TEM and found to be 2.6 ± 0.3, 6.1 ± 0.7, and 14.8 ± 1.8 nm (Figure 1A). We used X-ray diffraction to further investigate the size of the nanoparticles. From the XRD patterns, all of the AuNPs could be indexed to the cubic form of Au with a PDF number of 04−0784 (cubic, $a = b = c = 0.2884$ nm, $d(111) = 0.2355$ nm). As shown in Figure 1D, five primary diffraction peaks were observed, with peak angles of 38.187, 44.385, 64.576, 77.567, and 81.722, which corresponded to crystal plane indexes of (111), (200), (220), (311), and (222) for Au.[22] Further observations showed that each peak was wider than that of the corresponding bulk material, which is a characteristic property of nanocrystal materials. According to the Scherrer formula, the smaller the size of the particle, the wider the corresponding XRD peak. The overall calculation based on the (111) peak line-width at half-maximum intensity roughly showed that the average sizes of the nanoparticles were about 2, 6, and 15 nm.

The visible absorption spectrum is correlated with shape, size, monodispersion, and surface stabilization of the AuNPs. Generally, as gold nanoparticles increase in size, the corresponding surface plasmon resonance peaks will shift toward longer wavelengths. This phenomenon was observed when we measured the 2, 6, and 15 nm nanoparticles: their corresponding wavelengths shifted to 505, 517, and 523 nm, respectively (Figure 1C). XPS in Figure 1E indicates that the molar ratio of S to Au in 2.6 nm Au@tiopronin NPs is 0.72, that in 6.1 nm Au@tiopronin NPs is 0.485, and that in 14.8 nm Au@tiopronin NPs is 0.224, respectively. Hence, the number of tiopronin per NPs is 392 for 2.6 nm AuNPs, 3248 for 6.1 nm AuNPs, and 22 523 for 14.8 nm AuNPs. In addition, the surface density of tiopronin in AuNPs was calculated to be 19 for 2.6 nm AuNPs, 29 for 6.1 nm AuNPs, and 32 for 14.8 nm AuNPs (the calculation method of the number and surface

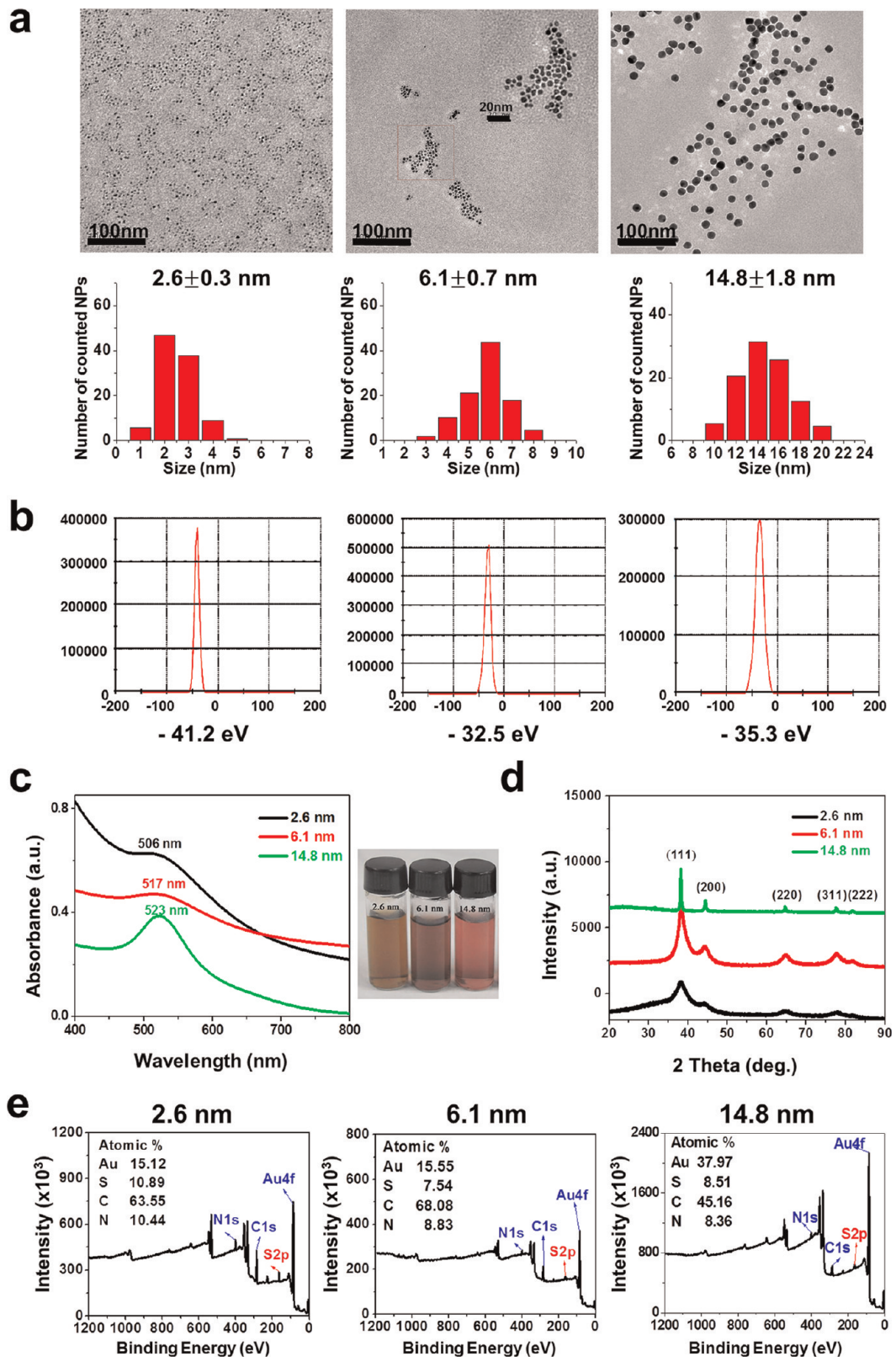

Figure 1. Characterization of 2, 6, and 15 nm gold nanoparticles with the same surface modification. (a) TEM images and corresponding size measurements of synthesized tiopronin coated Au nanopartices (Au@tiopronin NPs). Scale bars are 100 nm; the middle panel contains an additional scale bar of 20 nm. (b) Zeta-potential of the nanoparticles ranging from −32 to −41 eV. (c) Spectrum of the nanoparticles at wavelengths between 400 and 800 nm and corresponding photographs of the Au@tiopronin NPs dispersed in pure water. (d) XRD patterns of the synthesized Au@tiopronin NPs. (e) XPS graphs of the Au@tiopronin NPs.

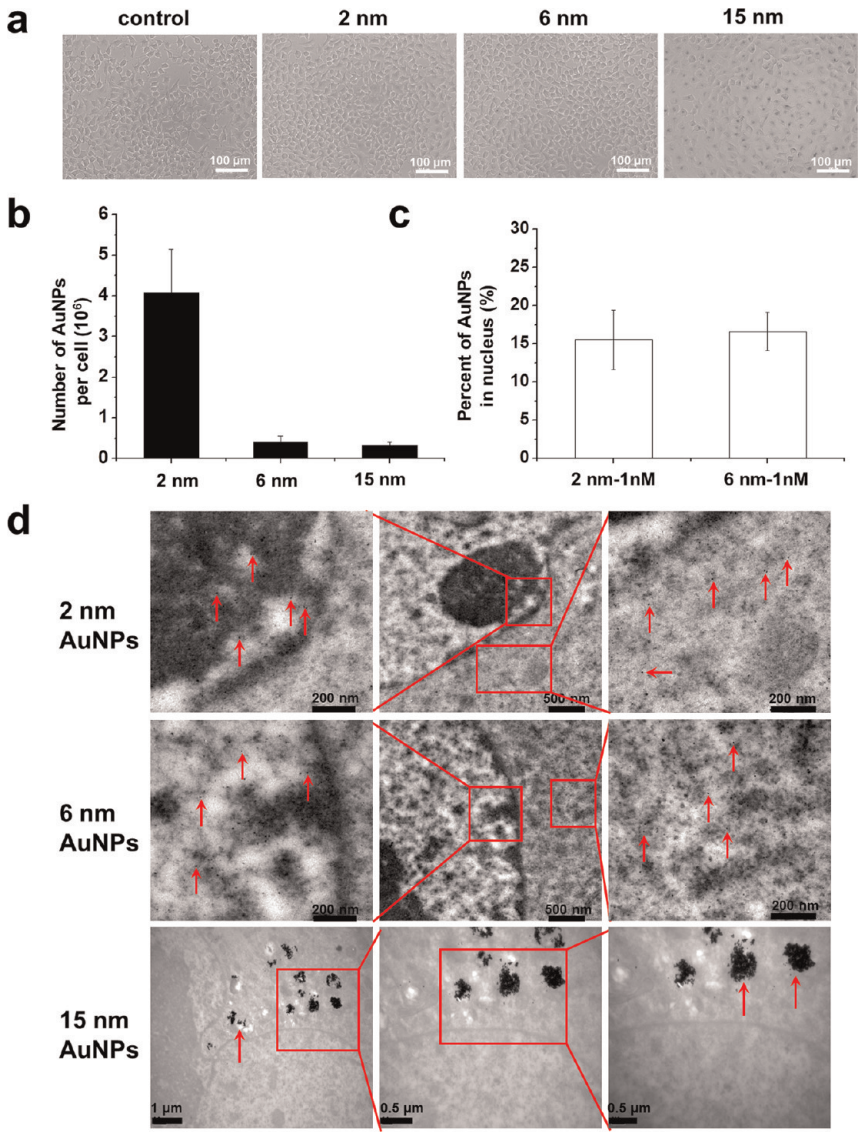

Figure 2. Uptake of 2, 6, and 15 nm AuNPs by MCF-7 monolayer cells. (a) Bright field images of cells after treatment with 1 nM gold nanoparticles for 24 h. (b) Quantitative ICP-MS measurement of AuNP uptake by cells treated as in (a). (c) Percentage of gold nanoparticles localized in the nucleus compared to the whole cell after treatment with 2 and 6 nm Au nanoparticles at 1 nM. (d) TEM images of cells treated with 1 nM nanoparticles for 24 h. Red arrows indicate the gold nanoparticles. Boxed regions are enlarged in the adjacent panels.

density of tiopronins per AuNPs is given in the Supporting Information).

We found that the AuNPs are water-soluble, well-dispersed in size, spherical in shape, and stable for more than one month without any aggregation. More importantly, all the nanoparticles have similar charges with a zeta-potential between −30 and −40 eV (Figure 1B). Thus, the only difference among the nanoparticles used in our study was the size.

Uptake of AuNPs by Monolayer Cancer Cells. It has recently been reported that the cellular uptake of nanoparticles ranging from 15 to 100 nm depends on size.[10,27,28] However, there is no detailed information about the uptake of nanoparticles that are smaller than 10 nm. We first evaluated the uptake of gold nanoparticles ranging from 2 to 15 nm by monolayer breast cancer cells.

The concentration of AuNPs was determined by calculating the gold atom concentration through ICP-MS measurements.[27] Cell viability was determined by CCK-8 assay, which showed that exposure to AuNPs for 24 h was not toxic to MCF-7 cells (Figure S3). This suggests good biocompatibility of ultrasmall AuNPs.

We then performed microscopic observation of different-sized AuNPs in the cells. Uptake of 15 nm AuNPs was clearly observed, but for 2 and 6 nm AuNPs, no obvious uptake was seen under light microscopy (Figure 2A). However, after quantitative analysis by ICP-MS, the profile of the number *versus* the size of gold nanoparticles in each cell indicated that uptake occurred in a size-dependent manner when cells were treated with 1 nM nanoparticles for 24 h. Nanoparticles of 2 nm showed higher cellular uptake than both 6 and

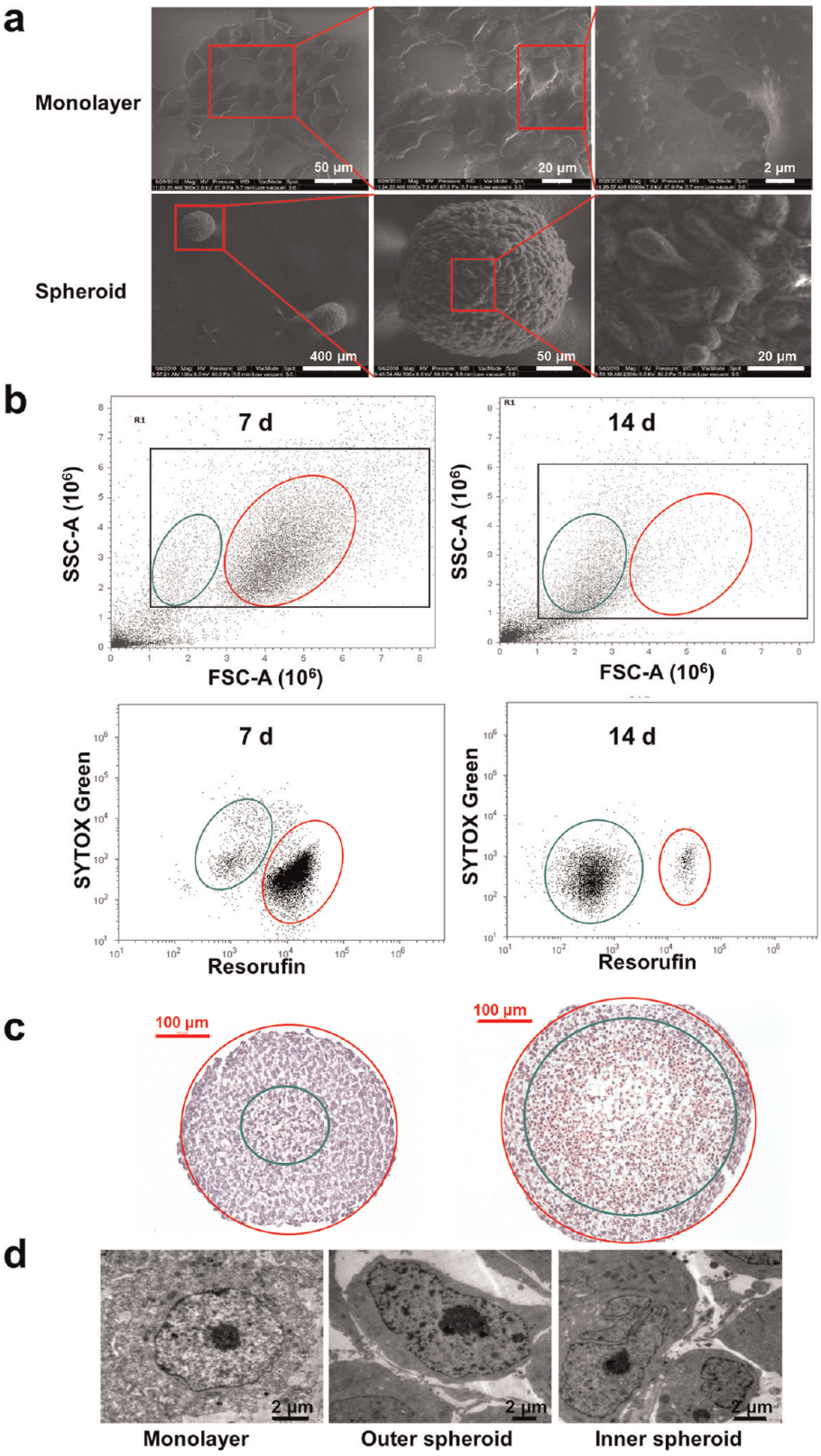

Figure 3. Characterization of MCF-7 monolayers and multicellular spheroids. (a) Bio-SEM of monolayer cells and 7-day-old spheroids seeded at a concentration of 600 cells per well. (b) Flow cytometry analysis of cell populations within 7- and 14-day-old spheroids seeded at a concentration of 600 cells per well. (c) Images of 7- and 14-day-old spheroids after HE staining. Apoptotic cells are located within the green circle, while proliferative cells are located between the green circle and the red circle. (d) TEM images of MCF-7 monolayer cells and of cells in the outer and inner regions of 14-day-old spheroids.

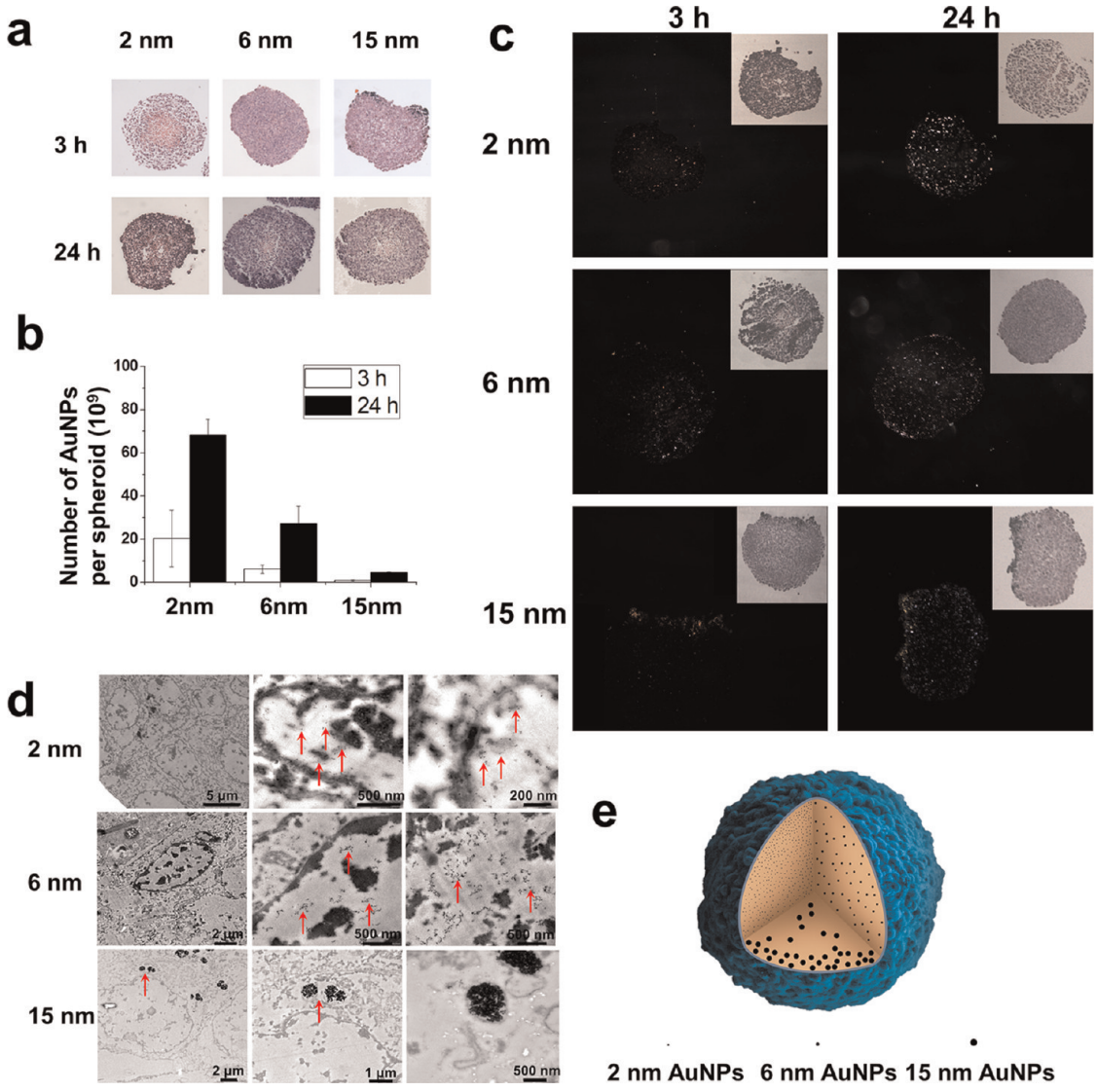

Figure 4. Penetration of 1 nM AuNPs into tumor spheroids after treatment for 3 and 24 h. (a) Images of spheroids treated with nanoparticles of different sizes after HE staining. (b) ICP-MS analysis of the number of Au nanoparticles in each treated spheroid. (c) Dark field images of spheroids after culture with nanoparticles of different sizes. (d) Representative TEM images of the external and internal regions of spheroids treated for 24 h. Red arrows indicate the gold nanoparticles. (e) Schematic illustration of the penetration behavior of AuNPs of different sizes.

15 nm nanoparticles, which might be due to their ultrasmall structure (Figure 2B). Previously, it had been reported that 50 nm citrate-stabilized gold nanoparticles were taken up at a higher concentration than were nanoparticles of other sizes (15−100 nm).[27] We treated MCF-7 cells resistant to doxorubicin (MCF-7R) with 0.5 nM 2, 6, and 15 nm AuNPs for 24 h and found a similar size-dependent uptake (Figure S4). Recently, several studies have reported that the cellular uptake of nanoparticles depends on many factors, including the size[27,29] or shape[30−32] of the nanoparticles, surface charge,[5,33,34] sedimentation and diffusion velocity effects of large and dense particles,[35] composition of the protein corona on the nanoparticles,[36] competition between receptors and ligands,[12,37] and the stage of the cell cycle.[38]

Localization of Au NPs in Monolayer Cancer Cells. We were surprised to observe localization of the 2 and 6 nm AuNPs in both the cytoplasm and the nucleus, as shown by TEM images. In addition, the nanoparticles were evenly distributed in the cells without any aggregation (Figure 2D). It is well known that the nuclear pore size exclusion limit for the passive diffusion of macromolecules is about 9 nm.[39] We speculated that since these small AuNPs can clearly penetrate the nuclear membrane, they may be entering the nucleus through the nuclear pores. This is in agreement with the nuclear penetration of PEG-modified Au nanoparticles with a diameter of 3.7 nm.[40] In contrast, the 15 nm AuNPs did not enter the nucleus (Figure 2D). This might be due to nonspecific adsorption of serum proteins that mediate endocytosis.[10,27]

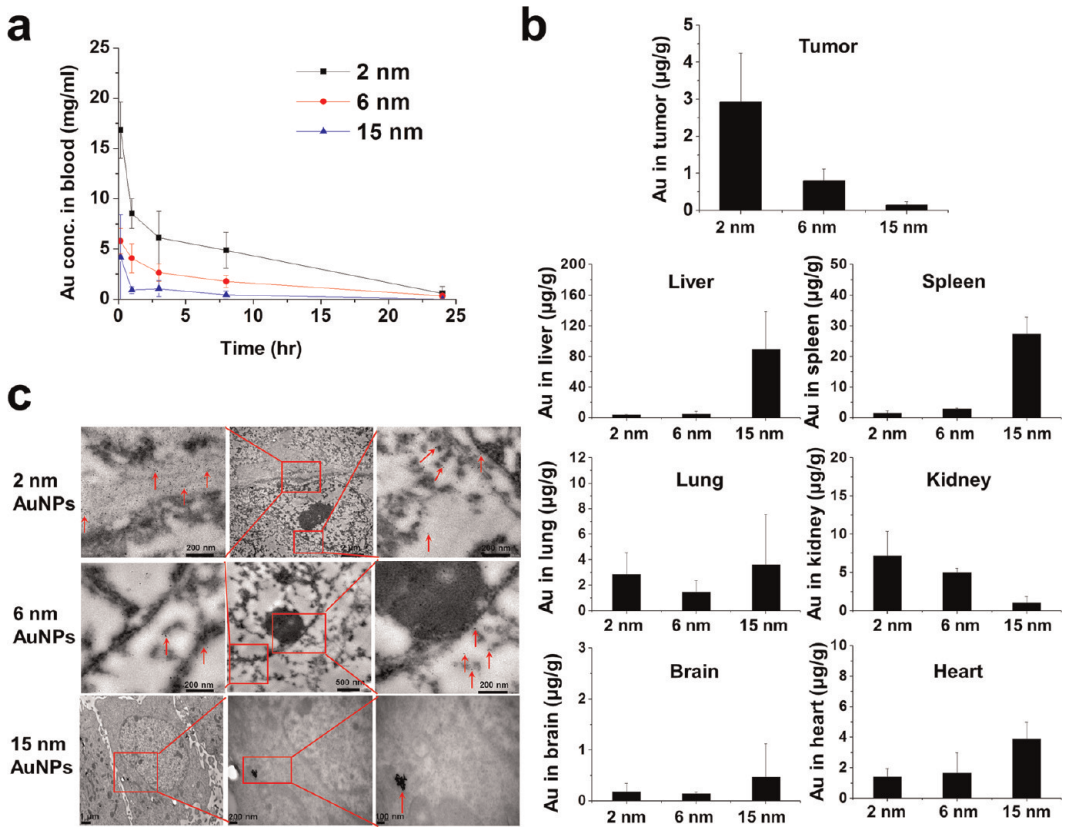

Figure 5. Pharmacokinetics and biodistribution of 2, 6, and 15 nm AuNPs. (a) Blood elimination profiles of Au following a single intravenous injection of Au nanoparticles at a dose of 5 mg Au/kg in tumor-bearing mice. Data represent mean ± SD ($n = 3$). (b) Au content in tumor, heart, liver, spleen, lung, brain, and kidney 24 h after iv injections of gold nanoparticles at 5 mg Au/kg. Data represent mean ± SD ($n = 3$) (c) Representative TEM micrographs of tumor tissue taken 24 h after the administration of AuNPs.

In order to confirm whether the 2 and 6 nm AuNPs were able to enter the nuclei of the cancer cells, we performed a quantitative study. Cell nuclei were extracted after 24 h treatment, and the percentage of Au nanoparticles in the nucleus was calculated. The percentage of Au nanoparticles in the nucleus was 15.5% for 2 nm nanoparticles and 16.6% for 6 nm nanoparticles (Figure 2C). These smaller AuNPs (2 and 6 nm) may possibly enter the cell by free diffusion like small molecules.

Establishment and Characterization of Multicellular MCF-7 Spheroids. Multicellular tumor spheroids, one of the most widely used three-dimensional (3D) culture systems, are proven to have many advantages over two-dimensional (2D) culture for cancer research because they resemble many aspects of the patho-physiological conditions within human tumor tissue.[3,22−24] We therefore developed spheroids of MCF-7 breast cancer cells as an *ex vivo* tumor model. Morphological analysis by SEM demonstrated that the MCF-7 cells formed tightly packed, rounded spheroids (Figure 3A). Within the spheroid, the cells were spindle-shaped and connections between the cells were very close and compact. This is similar to *in vivo* tumor tissue, but different from monolayer cells.

To further check the cell conditions in the tumor spheroids, flow cytometry analysis, HE staining, and TEM were performed. The data indicated that cells in 7-day-cultured spheroids could be divided into two groups (Figure 3B and C). One group included larger metabolically active cells, which were stained red by C12-resazurin in a vitality assay. These cells mainly localized to the outer part of the spheroid, as judged by HE staining. Another group included smaller apoptotic cells, which stained weakly with SYTOX green and were mainly found in the center of the spheroid. Two cell populations were also observed in 14-day-cultured spheroids, although the proportion of apoptotic cells increased as the culture time increased from 7 days to 14 days. A TEM study was performed to further analyze the cellular microstructure of the spheroids, and it confirmed that cells near the surface were in a healthy condition, similar to cells in monolayer culture, while the cells in the middle of the spheroid were apoptotic or injured and showed obvious chromatin compaction and segregation, as well as nuclear fragmentation (Figure 3D).

These results suggested that multicellular tumor spheroids mimic the distribution of cells around blood vessels in tumor tissue *in vivo*.[23] The outer region of the spheroid corresponds to tumor tissue near the blood supply, where cells proliferate in the presence of sufficient oxygen and nutrients. The inner region of the spheroid is quite similar to tumor tissue far away from the blood supply, where cells experience

decreased oxygen and nutrients. It was reported that nanoparticles were able to diffuse from the periphery to the center of tumor cylindroids.[5] Although multicellular tumor spheroids have already been used for biomedical applications, to our knowledge there has been no detailed description of spheroid development or of the condition of the cells within the spheroid. On the basis of our data, we selected spheroids as a suitable model for evaluating the penetration behavior of AuNPs in tumor tissue.

Penetration and Localization of AuNPs in MCF-7 Tumor Spheroids. There was no obvious difference in morphology of the spheroids after treatment with the three sizes of AuNPs at 1 nM for 3 and 24 h, as compared to untreated control spheroids (Figure S5). HE staining was carried out in order to confirm the exact site of localization of the AuNPs in the spheroid. The 2 and 6 nm NPs were not observed in the spheroid due to their ultrasmall size (Figure 4A). The 15 nm nanoparticles were seen only around the surface of the spheroid (Figure 4A), presumably because their larger size hindered their penetration into the center. The Au content significantly increased with incubation time from 3 to 24 h for both the 2 and 6 nm AuNPs, but not for the 15 nm AuNPs (Figure 4B).

The 2 and 6 nm AuNPs were distributed throughout both inner and outer compartments of the spheroid, suggesting that small nanoparticles can penetrate deeply into the spheroid (Figure 4C and E). This was not the case with the larger, 15 nm particles. In addition, quantitative analysis of ICP-MS data demonstrated that the smaller the size, the greater the number of AuNPs detected in each spheroid. For 2 and 6 nm nanoparticles, the AuNP content in each spheroid increased as the incubation time was extended from 3 to 24 h (Figure 4B). This result is consistent with the previous report that smaller nanoparticles of 20 nm showed superior penetration behavior into the spheroid than the larger nanoparticles of 40, 100, and 200 nm.[7]

Using TEM imaging, we found that 2 and 6 nm Au nanoparticles were located in the outer and inner regions of each spheroid and in the cytoplasm and nucleus of individual cells. These results were similar to those for monolayer cells. In contrast, the 15 nm AuNPs were localized in a few cell layers, mainly near the surface of the spheroid, and were found only in the cytoplasm of each cell (Figure 4D).

Accumulation of AuNPs in Tumor Tissue after Intravenous Injections. Size is an important parameter in the biological environment. It is well known that several kinds of nanoparticles around 100 nm in diameter are useful for drug delivery due to their enhanced permeation and retention (EPR) effect. Previous work has shown that these nanoparticles were usually distributed around tumor blood vessels, and there was little penetration into the tumor parenchyma.[41] When drug-loaded polymeric micelles with diameters of 30, 50, 70, and 100 nm were tested for their antitumor effect in mice, only the 30 nm polymer micelles were found to penetrate pancreatic tumors.[8] Recently, a smart nanoparticle composed of quantum dots realized both the long circulation half-life needed for the EPR effect and deep tumor penetration.[9]

To evaluate the accumulation of the three different sizes of AuNPs in tumor tissue *in vivo*, we used tumor-bearing mice. The pharmacokinetic behavior of the AuNPs was investigated after a single intravenous injection at a dose of 5 mg Au/kg. All the nanoparticles were eliminated rapidly from the blood. For 2 nm AuNPs, the blood concentration of Au was 26.2 μg/mL at 10 min postinjection, 7.57 μg/mL at 8 h, and 0.94 μg/mL at 24 h. For 6 nm nanoparticles, the gold levels were 9.0 μg/mL at 10 min, 2.8 μg/mL at 8 h, and 0.51 μg/mL at 24 h. Nanoparticles of 15 nm were cleared even more quickly from the blood (Figure 5A). In this work, all the AuNPs were coated with tiopronin. Hence, it is understandable that the nanoparticles were easily opsonized by the proteins and subsequently cleared from the blood. In order to effectively improve the circulation time of AuNPs, poly(ethylene glycol) (PEG) was conjugated to the gold nanoparticles to provide a stable brush layer.[42]

The amount of Au in tumor tissue 24 h after administration was 2.93 μg/g for 2 nm nanoparticles, 0.79 μg/g for 6 nm nanoparticles, and 0.14 μg/g for 15 nm nanoparticles (Figure 5B). On the basis of the above results, it is speculated that the smaller nanoparticles extravasate easily and diffuse away from the vessels with minimal hindrance. In contrast, the larger nanoparticles may extravasate and mainly localize at the perivascular space caused by the tumor microenvironment such as the extracellular matrix and interstitial fluid pressure. In order to take advantage of the superior penetration behavior of smaller size nanoparticles into tumor tissue, functional nanoparticles that shrunk from 100 nm to 10 nm were developed to realize deep tumor penetration and high accumulation in tumor *in vivo*.[43] In addition, the delivery of small nanoparticles (diameter, 12 nm) was improved by vascular normalization in mammary tumors, while hindering the delivery of larger nanoparticles (diameter, 125 nm).[44] When we examined other tissues, we found that 2 and 6 nm AuNPs accumulated mainly in the kidney, with smaller amounts present in the liver and spleen. This is consistent with the distribution behavior of 1.9 nm AuNPs.[45,46] Over 70% of the injected dose of the 15 nm AuNPs accumulated in the liver and spleen. For all three sizes, only low levels of nanoparticles were found in the brain, lung, and heart. Compared to the 15 nm AuNPs, the 2 and 6 nm AuNPs were widely distributed in different organs of the body due to their ultrasmall structures. In addition, TEM analysis of tumor cells demonstrated that 2 and 6 nm AuNPs were distributed evenly throughout the nucleus and cytoplasm, whereas 15 nm AuNPs were located only in the cytoplasm and formed aggregates (Figure 5C).

Histological analysis revealed that the AuNPs had almost no effect on tissues including liver, spleen, kidney, lung, and heart after administration, which indicated good tissue biocompatibility of the AuNPs used in this work (Figure S7). This is consistent with the fact that gold nanoparticles with different sizes and shapes are currently being used for human health applications.[47]

CONCLUSIONS

Our work provides new insights into the way that ultrasmall AuNPs, ranging from 2 to 15 nm, penetrate and localize within cultured cancer cells, multicellular spheroids, and tumors *in vivo*. The 2 and 6 nm gold nanoparticles demonstrated unique advantages over larger nanoparticles in terms of tumor uptake and permeability. Accumulation of nanoparticles in the tumor spheroid model occurred in a size-dependent manner, with 2 and 6 nm AuNPs able to penetrate deeply into tumor tissue. In summary, this work showed how nanoparticles can be designed and functionalized to achieve high levels of accumulation in tumor tissue.

EXPERIMENTAL SECTION

Materials. Sodium borohydride (≥98.0%), gold(III) chloride trihydrate (≥99.9%, $HAuCl_4 \cdot 3H_2O$), trisodium citrate tribasic dihydrate (≥99.0%), and *N*-(2-mercaptopropionyl)glycine (Tiopronin, $C_5H_9O_3NS$) were purchased from Sigma-Aldrich (St Louis, USA). L(+)-Ascorbic acid (99%) was supplied by Acros (USA). Nitric acid and hydrogen peroxide of MOS grade were bought from the Beijing Chemical Reagents Institute (China). Standard stock solution of Au (1000 μg/mL) was obtained from the National Analysis Center for Iron and Steel, China. All chemicals were used without further purification, and Milli-Q water was used throughout this study.

Synthesis of 2 and 6 nm Au@tiopronin NPs. The procedure for gold nanoparticle synthesis was as reported.[26] Au@tiopronin NPs of 2 nm were prepared by dissolving gold(III) chloride trihydrate (0.15 g, 0.4 mmol) and *N*-(2-mercaptopropionyl)glycine (tiopronin, 0.19 g,1.2 mmol) in 20 mL of methanol/acetic acid (6:1), producing a ruby red solution. Sodium borohydrate (0.30 g, 8.0 mmol) in 7.5 mL of H_2O was added dropwise with rapid stirring. After continuous stirring for 2 h, a black suspension was formed, and the solvent was then removed under vacuum at 40 °C. The residues were dissolved in 20 mL of H_2O, the pH was adjusted to 1 by dropwise addition of 1 M HCl, and then the solution was dialyzed (dialysis membrane, Solarbio, MWCO = 8000−14 000) for 72 h against Milli-Q water, which was changed every 8 h. The resulting Au@tiopronin NPs were lyophilized and dried completely before further use. The method to prepare 6 nm Au@tiopronin was the same except that the amount of tiopronin was decreased to 0.021 g (0.13 mmol).

Synthesis of 15 nm Au@tiopronin NPs. A surface molecule exchange reaction was adopted to obtain 15 nm Au@tiopronin NPs. Au@citrate NPs of 15 nm were first prepared by the standard citrate reduction method.[48] Briefly, 0.5 mL of $HAuCl_4 \cdot 3H_2O$ solution (1%, w/v) in 50 mL of Milli-Q water was heated to boiling; then 1.5 mL of trisodium citrate tribasic dihydrate solution (1%, m/v) was added quickly with vigorous stirring. After the color change finished in 5 min, the solution was kept boiling for another 15−30 min and then allowed to cool to room temperature while stirring. Subsequently, the tiopronin replacement was performed while stirring at 40 °C for more than 48 h by mixing Au@citrate solution, prepared as described above, with an aqueous solution containing a large excess of tiopronin. The molar ratio of tiopronin was 20 times more than that of $HAuCl_4$ to ensure the complete replacement of citrate by tiopronin in AuNPs, as the binding affinity of tiopronin to AuNPs with the formation of a Au−S bond is stronger than the electrostatic interaction between AuNPs and citrate. After the reaction, 15 nm Au@tiopronin NPs were purified by centrifugation several times at 9000 rpm for 30 min to remove the unbound tiopronin and the citrate from the AuNPs.

Characterization of AuNPs. The morphology of the Au@tiopronin NPs was determined using a Tecnai G2 20 STWIN transmission electron microscope (TEM, Philips, Netherlands) with 200 kV acceleration voltage. Optical absorption spectra were measured with a Lambda 950 UV/vis/NIR spectrophotometer (Perkin-Elmer, USA). X-ray diffraction spectra and X-ray photoelectron spectra were tested separately with an X'Pert PRO MPD X-ray diffractometer (PANalytical B.V., The Netherlands) and an ESCALAB250Xi X-ray photoelectron spectrometer (Thermo Fisher Scientific, UK). Zeta-potential distribution of AuNPs was determined by a Zetasizer Nano ZS (Malvern, England), and the measurements were recorded at 25 °C suspended in Milli-Q water. The concentration of gold was determined *via* an Optima 5300DV inductively coupled plasma optical emission spectrometer or an ELAN DRC-e inductively coupled plasma mass spectrometer (Perkin-Elmer, USA).

Uptake of AuNPs by Monolayer Cells. The human breast cancer cell line MCF-7 was maintained in Dulbecco's modified Eagle's medium with 10% fetal bovine serum in a humidified atmosphere containing 5% CO_2 at 37 °C. MCF-7 cells were cultured in six-well plates at about 60% confluence. After 24 h incubation, the medium was removed and 1 mL of fresh medium containing 1 nM 2, 6, and 15 nm AuNPs was added to the wells. After 24 h, cells were washed gently with PBS, digested with 0.25% trypsin, centrifuged for 3 min at 1000 rpm, and then collected and counted by Vi-CELL (Beckman Coulter, USA).

Isolation of Cell Nuclei and Qualitative Determination of Au Content. MCF-7 cells were grown at about 60% confluence in six-well plates for 24 h. Afterward, 1 nM gold nanoparticles of 2 and 6 nm were added to the wells. After 24 h incubation, the cells were trypsinized, washed with PBS, and centrifuged for 3 min at 1000 rpm. The treated cells were then divided into two equal parts, one part for direct analysis by ICP-MS and the other for isolation of nuclei using a nuclear extraction kit (Solarbio, Shanghai, China). The percentage of Au nanoparticles in the nucleus was calculated according to the Au content in the isolated nuclei compared to the whole cells.

Cell Viability Assay. Cell viability was determined using the Cell Counting Kit-8 (CCK-8, Dojindo Laboratories, Japan). First, cells were seeded into 96-well plates (Costar, Corning, NY, USA). After incubation for 24 h, the culture medium was removed and replaced with complete medium containing 2 nm AuNPs at a dose from 4 to 411 nM, 6 nm AuNPs from 0.38 to 38 nM, and 14.8 nm AuNPs from 0.625 to 10 nM. Cells unexposed to Au nanoparticles were regarded as controls. Cell viability was calculated as the ratio of the absorbance of treated and control wells. The absorbance was measured at 450 nm with a reference wavelength of 650 nm using an Infinite M200 microplate reader (Tecan, Durham, NC, USA).

MCF-7 Multicelluar Spheroid Culture. MCF-7 spheroids were produced by the liquid overlay method as previously described.[49] Briefly, cells were detached from monolayers, and single cell suspensions (200 μL per well containing 600 cells) were transferred into flat-bottomed 96-well plates precoated with 1% agarose. Cells were incubated for about 7 days as described above for monolayer cells, except that the culture medium was partially (100 μL) replaced by fresh medium every other day.

SEM Observation of MCF-7 Tumor Spheroids. Environmental scanning electron microscopy was used to examine the outer morphology of the spheroid. After incubation for one week, the spheroids were removed from the wells, washed with PBS

(150 mM, pH 7.4), and fixed overnight at room temperature in 5% glutaraldehyde solution. The spheroids were then progressively dehydrated in an ethanol series from 70% to 100%, followed by critical point drying with isoamyl acetate. Finally, the spheroids (without gold coating) were observed by SEM (FEI Quanta 200). For monolayer cells, cells were cultured on coverslips for 24 h; then the medium was removed and the cells were treated in the same way as the spheroids.

Penetration of AuNPs into Spheroids. For 7-day-old spheroids seeded at a concentration of 600 cells per well, 100 μL of medium was replaced with 2 nM nanoparticles at a final concentration of 1 nM. After 24 h incubation, the spheroids were removed by pipet and gently washed with PBS. The distribution of AuNPs in the spheroid was qualitatively observed using bright field and dark field microscopy. The ultramicrolocalization of gold nanoparticles in the outer and inner cells of the spheroid was evaluated by TEM. In addition, the Au content in every spheroid was quantified by ICP-MS.

Pharmacokinetics and Biodistribution of AuNPs *in Vivo*. Female Balb/c nude mice (18−20 g) were purchased from Beijing Vital River Laboratories. All care and handling of animals were performed with the approval of the Animal Ethics Committee of the Medical School, Peking University. To establish tumor-bearing mice, animals were subcutaneously inoculated in the right flank with 4×10^6 MCF-7S cells. When the average volume of the tumors reached about 100 mm^3, the mice were divided randomly into groups for the pharmacokinetics and distribution studies.

For the pharmacokinetics study, tumor-bearing mice were intravenously injected with AuNPs of 2, 6, and 15 nm at a dose of 5 mg Au/kg. About 30−100 μL blood was taken from the tail vein with a quantitative capillary at 10 min, 1 h, 3 h, 8 h, and 24 h after administration. The nanoparticles were injected at the lower part of one tail vein, and the blood sample was taken at the other side of the tail vein, thereby protecting the sample from contamination. The blood volume was calculated as 0.0778 mL/g body weight. For the tissue distribution evaluation, tissues including tumor, heart, liver, spleen, lung, and kidney were removed 24 h after injection. The tissues were used for ICP-MS measurement, TEM observation, and histological evaluation. The blood and part of the tissue samples were used to quantitate the Au content by ICP-MS.

TEM Observation of Spheroids and Tumors. SEM observation was used to evaluate the morphology of the outer cells in the spheroid. In order to evaluate the inner cells of the spheroid, TEM was carried out. Briefly, 7-day-cultured spheroids were removed, washed with PBS, and fixed overnight at room temperature using 3% glutaraldehyde solution. This was followed by secondary fixation with 1% osmium tetraoxide, then serial dehydration in a graded ethanol series. Each spheroid was embedded in Epon resin and polymerized for 3 days at 60 °C. Embedded samples were sectioned, stained with uranyl acetate, and examined under an electron microscope (JEM-1400, JEOL). For tumor tissues, small pieces of the tumor were collected and processed as described for spheroids, except that the sections were not stained with uranyl acetate.

HE Staining. After the biodistribution study, tissue samples including tumor, heart, liver, spleen, lung, and kidney were collected and fixed in 4% formalin for at least one day. The samples were then dehydrated in an ethanol series, embedded in paraffin, and sectioned. Subsequently, sections were stained with hematoxylin and eosin (HE) according to the standard protocol.

ICP-MS Analysis. For the quantitative determination of Au content, cell samples, blood samples, and tissue samples were digested in aqua fortis composed of nitric acid and hydrochloric acid (3:1, v/v), diluted with 2% nitric acid and 1% hydrochloric acid, and then subjected to ICP-MS.

Conflict of Interest: The authors declare no competing financial interest.

Acknowledgment. This work was supported by Chinese Natural Science Foundation Project (Nos. 30970784, 81171455, and 31100720), National Key Basic Research Program of China (2009CB930200), Chinese Academy of Sciences (CAS) "Hundred Talents Program" (07165111ZX), and CAS Knowledge Innovation Program. The work was also partially supported by 2G12RR003048 from the RCMI Program and Tianjin Research Program of Applied Basic & Cutting-edge Technologies (No. 09JCYBJC27200).

Supporting Information Available: Characterization of the 15 nm Au@citrate NPs and Au@tiopronin NPs; visible absorption spectrum and XRD profile of the Au@citrate NPs and Au@tiopronin NPs; viability of MCF-7 cells after treatment with AuNPs of 2, 6, and 15 nm; cellular uptake of AuNPs of 2, 6, and 15 nm in MCF-7R cell lines; images of the MCF-7 tumor spheroids; pharmacokinetics of AuNPs after intravenous injection; images of tissues after HE staining; calculation of the number and the surface density of tiopronins per NP. This material is available free of charge *via* the Internet at http://pubs.acs.org.

REFERENCES AND NOTES

1. Gradishar, W. J.; Tjulandin, S.; Davidson, N.; Shaw, H.; Desai, N.; Bhar, P.; Hawkins, M.; O'Shaughnessy, J. Phase III Trial of Nanoparticle Albumin-Bound Paclitaxel Compared with Polyethylated Castor Oil-Based Paclitaxel in Women with Breast Cancer. *J. Clin. Oncol.* **2005**, *23*, 7794–7803.
2. Torchilin, V. P. Recent Advances with Liposomes as Pharmaceutical Carriers. *Nat. Rev. Drug Discovery* **2005**, *4*, 145–160.
3. Minchinton, A. I.; Tannock, I. F. Drug Penetration in Solid Tumours. *Nat. Rev. Cancer* **2006**, *6*, 583–592.
4. Mikhail, A. S.; Allen, C. Block Copolymer Micelles for Delivery of Cancer Therapy: Transport at the Whole Body, Tissue and Cellular Levels. *J. Controlled Release* **2009**, *138*, 214–223.
5. Kim, B.; Han, G.; Toley, B. J.; Kim, C. K.; Rotello, V. M.; Forbes, N. S. Tuning Payload Delivery in Tumour Cylindroids Using Gold Nanoparticles. *Nat. Nanotechnol.* **2010**, *5*, 465–472.
6. Chauhan, V. P.; Popovic, Z.; Chen, O.; Cui, J.; Fukumura, D.; Bawendi, M. G.; Jain, R. K. Fluorescent Nanorods and Nanospheres for Real-Time in Vivo Probing of Nanoparticle Shape-Dependent Tumor Penetration. *Angew. Chem., Int. Ed.* **2011**, *50*, 11417–11420.
7. Goodman, T. T.; Olive, P. L.; Pun, S. H. Increased Nanoparticle Penetration in Collagenase-Treated Multicellular Spheroids. *Int. J. Nanomed.* **2007**, *2*, 265–274.
8. Cabral, H.; Matsumoto, Y.; Mizuno, K.; Chen, Q.; Murakami, M.; Kimura, M.; Terada, Y.; Kano, M. R.; Miyazono, K.; Uesaka, M. Accumulation of Sub-100 nm Polymeric Micelles in Poorly Permeable Tumours Depends on Size. *Nat. Nanotechnol.* **2011**, *6*, 815–823.
9. Wong, C.; Stylianopoulos, T.; Cui, J. A.; Martin, J.; Chauhan, V. P.; Jiang, W.; Popovic, Z.; Jain, R. K.; Bawendi, M. G.; Fukumura, D. Multistage Nanoparticle Delivery System for Deep Penetration into Tumor Tissue. *Proc. Natl. Acad. Sci. U. S. A.* **2011**, *108*, 2426–2431.
10. Jiang, W.; Kim, B. Y. S.; Rutka, J. T.; Chan, W. C. W. Nanoparticle-Mediated Cellular Response Is Size-Dependent. *Nat. Nanotechnol.* **2008**, *3*, 145–150.
11. Cobley, C. M.; Chen, J. Y.; Cho, E. C.; Wang, L. V.; Xia, Y. N.; Gold Nanostructures, A Class of Multifunctional Materials for Biomedical Applications. *Chem. Soc. Rev.* **2011**, *40*, 44–56.
12. Kumar, A.; Ma, H. L.; Zhang, X.; Huang, K. Y.; Jin, S. B.; Liu, J.; Wei, T.; Cao, W. P.; Zou, G. Z.; Liang, X. J. Gold Nanoparticles Functionalized with Therapeutic and Targeted Peptides for Cancer Treatment. *Biomaterials* **2012**, *33*, 1180–1189.
13. Duncan, B.; Kim, C.; Rotello, V. M. Gold Nanoparticle Platforms as Drug and Biomacromolecule Delivery Systems. *J. Controlled Release* **2010**, *148*, 122–127.
14. Paciotti, G. F.; Myer, L.; Weinreich, D.; Goia, D.; Pavel, N.; McLaughlin, R. E.; Tamarkin, L. Colloidal Gold: A Novel Nanoparticle Vector for Tumor Directed Drug Delivery. *Drug Delivery* **2004**, *11*, 169–183.
15. Libutti, S. K.; Paciotti, G. F.; Byrnes, A. A.; Alexander, H. R., Jr.; Gannon, W. E.; Walker, M.; Seidel, G. D.; Yuldasheva, N.; Tamarkin, L.; Phase, I and Pharmacokinetic Studies of Cyt-6091, a Novel Pegylated Colloidal Gold-Rhtnf Nanomedicine. *Clin. Cancer Res.* **2010**, *16*, 6139–6149.

16. Zhao, Y.; Tian, Y.; Cui, Y.; Liu, W.; Ma, W.; Jiang, X. Small Molecule-Capped Gold Nanoparticles as Potent Antibacterial Agents That Target Gram-Negative Bacteria. *J. Am. Chem. Soc.* **2010**, *132*, 12349–12356.
17. Wang, F.; Wang, Y. C.; Dou, S.; Xiong, M. H.; Sun, T. M.; Wang, J. Doxorubicin-Tethered Responsive Gold Nanoparticles Facilitate Intracellular Drug Delivery for Overcoming Multidrug Resistance in Cancer Cells. *ACS Nano* **2011**, *5*, 3679–3692.
18. Shaw, C. P.; Middleton, D. A.; Volk, M.; Levy, R. Amyloid-Derived Peptide Forms Self-Assembled Monolayers on Gold Nanoparticle with a Curvature-Dependent Beta-Sheet Structure. *ACS Nano* **2012**, *6*, 1416–1426.
19. Rosi, N. L.; Giljohann, D. A.; Thaxton, C. S.; Lytton-Jean, A. K.; Han, M. S.; Mirkin, C. A. Oligonucleotide-Modified Gold Nanoparticles for Intracellular Gene Regulation. *Science* **2006**, *312*, 1027–1030.
20. Giljohann, D. A.; Seferos, D. S.; Patel, P. C.; Millstone, J. E.; Rosi, N. L.; Mirkin, C. A. Oligonucleotide Loading Determines Cellular Uptake of DNA-Modified Gold Nanoparticles. *Nano Lett.* **2007**, *7*, 3818–3821.
21. Massich, M. D.; Giljohann, D. A.; Schmucker, A. L.; Patel, P. C.; Mirkin, C. A. Cellular Response of Polyvalent Oligonucleotide-Gold Nanoparticle Conjugates. *ACS Nano* **2010**, *4*, 5641–5646.
22. Ong, S. M.; Zhao, Z.; Arooz, T.; Zhao, D.; Zhang, S.; Du, T.; Wasser, M.; van Noort, D.; Yu, H. Engineering a Scaffold-Free 3D Tumor Model for in Vitro Drug Penetration Studies. *Biomaterials* **2010**, *31*, 1180–1190.
23. Lin, R. Z.; Chang, H. Y. Recent Advances in Three-Dimensional Multicellular Spheroid Culture for Biomedical Research. *Biotechnol. J* **2008**, *3*, 1172–1184.
24. Pickl, M.; Ries, C. H. Comparison of 3D and 2D Tumor Models Reveals Enhanced Her2 Activation in 3D Associated with an Increased Response to Trastuzumab. *Oncogene* **2009**, *28*, 461–468.
25. Goldsborough, A. S.; Handley, M. D.; Dulcey, A. E.; Pluchino, K. M.; Kannan, P.; Brimacombe, K. R.; Hall, M. D.; Griffiths, G.; Gottesman, M. M. Collateral Sensitivity of Multidrug-Resistant Cells to the Orphan Drug Tiopronin. *J. Med. Chem.* **2011**, *54*, 4987–4997.
26. Templeton, A. C.; Chen, S. W.; Gross, S. M.; Murray, R. W. Water-Soluble, Isolable Gold Clusters Protected by Tiopronin and Coenzyme a Monolayers. *Langmuir* **1999**, *15*, 66–76.
27. Chithrani, B. D.; Ghazani, A. A.; Chan, W. C. W. Determining the Size and Shape Dependence of Gold Nanoparticle Uptake into Mammalian Cells. *Nano Lett.* **2006**, *6*, 662–668.
28. Chithrani, B. D.; Chan, W. C. Elucidating the Mechanism of Cellular Uptake and Removal of Protein-Coated Gold Nanoparticles of Different Sizes and Shapes. *Nano Lett.* **2007**, *7*, 1542–1550.
29. Zhang, S. L.; Li, J.; Lykotrafitis, G.; Bao, G.; Suresh, S. Size-Dependent Endocytosis of Nanoparticles. *Adv. Mater.* **2009**, *21*, 419–424.
30. Chithrani, B. D.; Stewart, J.; Allen, C.; Jaffray, D. A. Intracellular Uptake, Transport, and Processing of Nanostructures in Cancer Cells. *Nanomedicine* **2009**, *5*, 118–127.
31. Cho, E. C.; Au, L.; Zhang, Q.; Xia, Y. N. The Effects of Size, Shape, and Surface Functional Group of Gold Nanostructures on Their Adsorption and Internalization by Cells. *Small* **2010**, *6*, 517–522.
32. Gratton, S. E. A.; Ropp, P. A.; Pohlhaus, P. D.; Luft, J. C.; Madden, V. J.; Napier, M. E.; DeSimone, J. M. The Effect of Particle Design on Cellular Internalization Pathways. *Proc. Natl. Acad. Sci. U. S. A.* **2008**, *105*, 11613–11618.
33. He, C. B.; Hu, Y. P.; Yin, L. C.; Tang, C.; Yin, C. H. Effects of Particle Size and Surface Charge on Cellular Uptake and Biodistribution of Polymeric Nanoparticles. *Biomaterials* **2010**, *31*, 3657–3666.
34. Verma, A.; Uzun, O.; Hu, Y. H.; Hu, Y.; Han, H. S.; Watson, N.; Chen, S. L.; Irvine, D. J.; Stellacci, F. Surface-Structure-Regulated Cell-Membrane Penetration by Monolayer-Protected Nanoparticles. *Nat. Mater.* **2008**, *7*, 588–595.
35. Cho, E. C.; Zhang, Q.; Xia, Y. N. The Effect of Sedimentation and Diffusion on Cellular Uptake of Gold Nanoparticles. *Nat. Nanotechnol.* **2011**, *6*, 385–391.
36. Cedervall, T.; Lynch, I.; Lindman, S.; Berggard, T.; Thulin, E.; Nilsson, H.; Dawson, K. A.; Linse, S. Understanding the Nanoparticle-Protein Corona Using Methods to Quantify Exchange Rates and Affinities of Proteins for Nanoparticles. *Proc. Natl. Acad. Sci. U. S. A.* **2007**, *104*, 2050–2055.
37. Maus, L.; Dick, O.; Bading, H.; Spatz, J. P.; Fiammengo, R. Conjugation of Peptides to the Passivation Shell of Gold Nanoparticles for Targeting of Cell-Surface Receptors. *ACS Nano* **2010**, *4*, 6617–6628.
38. Kim, J. A.; Aberg, C.; Salvati, A.; Dawson, K. A. Role of Cell Cycle on the Cellular Uptake and Dilution of Nanoparticles in a Cell Population. *Nat. Nanotechnol.* **2012**, *7*, 62–68.
39. Paine, P. L.; Moore, L. C.; Horowitz, S. B. Nuclear-Envelope Permeability. *Nature* **1975**, *254*, 109–114.
40. Gu, Y. J.; Cheng, J.; Lin, C. C.; Lam, Y. W.; Cheng, S. H.; Wong, W. T. Nuclear Penetration of Surface Functionalized Gold Nanoparticles. *Toxicol. Appl. Pharmacol.* **2009**, *237*, 196–204.
41. Matsumura, Y.; Maeda, H. A New Concept for Macromolecular Therapeutics in Cancer-Chemotherapy - Mechanism of Tumoritropic Accumulation of Proteins and the Antitumor Agent Smancs. *Cancer Res.* **1986**, *46*, 6387–6392.
42. Perrault, S. D.; Walkey, C.; Jennings, T.; Fischer, H. C.; Chan, W. C. Mediating Tumor Targeting Efficiency of Nanoparticles through Design. *Nano Lett.* **2009**, *9*, 1909–1915.
43. Wong, C.; Stylianopoulos, T.; Cui, J.; Martin, J.; Chauhan, V. P.; Jiang, W.; Popovic, Z.; Jain, R. K.; Bawendi, M. G.; Fukumura, D. Multistage Nanoparticle Delivery System for Deep Penetration into Tumor Tissue. *Proc. Natl. Acad. Sci. U. S. A.* **2011**, *108*, 2426–2431.
44. Chauhan, V. P.; Stylianopoulos, T.; Martin, J. D.; Popovic, Z.; Chen, O.; Kamoun, W. S.; Bawendi, M. G.; Fukumura, D.; Jain, R. K. Normalization of Tumour Blood Vessels Improves the Delivery of Nanomedicines in a Size-Dependent Manner. *Nat. Nanotechnol.* **2012**, DOI: 10.1038/NNANO.2012.45.
45. Hirn, S.; Semmler-Behnke, M.; Schleh, C.; Wenk, A.; Lipka, J.; Schaffler, M.; Takenaka, S.; Moller, W.; Schmid, G.; Simon, U. Particle Size-Dependent and Surface Charge-Dependent Biodistribution of Gold Nanoparticles after Intravenous Administration. *Eur. J. Pharm. Biopharm.* **2011**, *77*, 407–416.
46. Hainfeld, J. F.; Slatkin, D. N.; Focella, T. M.; Smilowitz, H. M. Gold Nanoparticles: A New X-Ray Contrast Agent. *Br. J. Radiol.* **2006**, *79*, 248–253.
47. Sperling, R. A.; Rivera gil, P.; Zhang, F.; Zanella, M.; Parak, W. J. Biological Applications of Gold Nanoparticles. *Chem. Soc. Rev.* **2008**, *37*, 1896–1908.
48. Frens, G. Controlled Nucleation for Regulation of Particle-Size in Monodisperse Gold Suspensions. *Nat. Phys. Sci.* **1973**, *241*, 20–22.
49. Friedrich, J.; Seidel, C.; Ebner, R.; Kunz-Schughart, L. A. Spheroid-Based Drug Screen: Considerations and Practical Approach. *Nat. Protoc.* **2009**, *4*, 309–324.